Mechanical Engineering Advances 2024, 2(2), 1633.
https://doi.org/10.59400/mea.v2i2.1633

Article

Reliability, sustainability, resiliency, and performance investigation of an embedded splice-sleeve connector at high velocity semi-trailer impact

Suman Roy

Department of Civil and Environmental Engineering, Utah State University, Logan, UT 84322, USA; sumanroy74@gmail.com

CITATION

Roy S. Reliability, sustainability, resiliency, and performance investigation of an embedded splice-sleeve connector at high velocity semi-trailer impact. Mechanical Engineering Advances. 2024; 2(2): 1633. https://doi.org/10.59400/mea.v2i2.1633

ARTICLE INFO

Received: 22 April 2024
Accepted: 25 June 2024
Available online: 20 July 2024

Abstract: Presently, dynamic impacts occurrences caused by car crashes have been frequently reported. Statistical results from different articles indicate that vehicle crashworthiness of bridge pier supersedes the other events. However, majority of the published articles focusses on sustainability and finding severity of distressed pier due to impact correlating faster construction methods, like accelerated bridge construction (ABC). This article is an attempt to examine post impacted behavior of a commonly used connector in ABC for resisting short duration shock. Static and dynamic performance analyses of a connector embedded within a coupler system has been examined. A representative ABC pier with the standardized and selected material properties collected from manufacturer's data has been utilized. Coupler composite materials consisting of a hollow uniform cross-section cast iron cylinder filled up with specified concrete grout conforms higher strength. The performance examination has been conducted by numerical modeling using finite element method (FEM). A commercially used software ANSYS has been utilized for carrying out the simulations. To investigate the post impact dynamic behavior, mesh-independent studies seems inevitable and hence are executed to evaluate dynamic impact factor (DIF). Sensitivity studies are carried out for validating results in precision. The DIF of the main reinforcing tensile steel embedded into the grout placed inside the connector has been determined. Results captured from simulations to identify material properties at plastic stage in sustaining such load have been conducted. The results provide significant information that aids opting for selecting suitable connectors for attaining help the design offices.

Keywords: non-traditional bridge pier; semi-trailer impact; connector; FEM and its validity

1. Introduction

Increased occurrences of dynamic impact caused by high strain rate loading warrants structural viability that intimidates serviceability, resilience, and reliability. Reinforced concrete (RC) bridge piers primarily receive various short duration impact loads caused by earthquake, blast, and car crash. All these loads being short duration impact may cause performance degradation from less severe to pier dislocation. High seismicity being considered in the western United States of America (USA) has received adequate attention to examine structural feasibility [1]. Traditional RC bridge piers responding at higher seismic loads has been the subject of interests by many researchers from years. To improve the post impact behavior of such piers by resisting damage during medium to devastating earthquakes, adequate research was carried out to assess various damage levels. Blast resistant design of structures has been carried out by many researchers as well [2]. On the other hand, high strain rate impact loads exerted by vehicular collision creates quite complex mechanisms comprising uncertainty caused by relatively unknown vehicle bridge-pier interaction and failure mechanism. However, this area of structural investigations has received limited

attention. So, an additional insightful study is required for RC bridge pier performance at short duration high strain rate load. High velocity vehicle crash as exerts higher strain rate force at high-speed hit on bridge pier, frontal overpressure due to contact for collision can result certain damage levels from concrete spalling to cracking [3]. Recently published articles in various journals corroborated that the car crashes with bridge elements most likely to be occurred with the rising number of vehicles [4]. The post-crash behavior of the coupler composite incurred by high velocity vehicle impact has been investigated. Results in terms of stresses are captured at the highly possible susceptible region to estimate plastic deformation. Different high strain rates dynamic loads instilled at tensile steel bar of traditional RC pier were analyzed, and the evaluated results were published for both flexure and combined stresses [5]. Different studies corroborate that damage characterization experienced by impact load is not only the function of reinforcing steel but highly dependent on the strength of concrete. Combination of different parameters controlling post impact pier behavior endorses a fairly good agreement between withstanding the transverse load resisting capacity as a primary mechanism followed by the flexural capacity that governs principal serviceability to resist post impact distresses in bridge pier [6].

Dynamic load exhibited on connectors used in the non-traditional ABC bridge pier also warrants an insightful investigation and hence demand rigorous estimation of performance at dynamic load. This present context will help to precisely scrutinize the material behavior and the post impact response of such connectors at high velocity crash load incurred by semi-trailer hit by using uncertainty variables controlling performance level. Adequate investigation due to a high frequency of occurrence of vehicle impact on ABC pier warrants precise attention [7]. This has been recently observed that crashworthiness of pier direly reduces the health, and hence calls for serviceability. The prevalence of the present research studies is carried out to identify various damage levels or increasing survivability [8,9]. On the other hand, connectors such as splice sleeves and high strength grout used in ABC system are commonly used as connectors assembling different bridge components such as beam elements and piers along with the foundations needs additional inspection. Permanent hinges due to large plastic deformation are predicted to be formed in the fragile part of the structural element, envisaging substantial amount of energy dissipation [10]. The introduction of new materials used as connectors in terms of splice sleeves and grouted couplers in withstanding the dynamic load differs from traditional RC pier in a manner that they are expected to behave like higher stiffness's than a single reinforcing bar although the discontinuities of the bar at 'Rebar Stop' takes place to change the energy dissipation path at connector [10,11]. In addition, connectors in order to facilitate the construction method of bridge, formation of the plastic hinge at short duration impact requires rigorous scrutinization. However, this is restricted with the consideration of seismic as specified in the bridge design codes by [12]. Additionally, investigating newer construction methods using connectors, various performance at impacts and their damage levels needs to be assessed under multi-hazard load effects. The combination of sequential loads by virtue of blast and car crash have already been discussed for traditional RC pier using resistance reduction method (RRM).

In performing an explicit evaluation of the post impact behavior of coupler system utilized in ABC needs to be scrutinized. In this present study, geometries of

pier proposed by Utah Department of Transportation (UDOT) [12] has been considered and examined for studies. The connectors' details were extracted from manufacturer's data furnished by NMB splice sleeve needs an additional attention. To precisely depict the crash performance of connector, it is placed in the pier- foundation junction. Connectors are embedded in the foundation to understand the complex mechanism as predicted by the composite material's interactive action [13] has further been studied and the report was published by 'Idaho Transportation Department'. In addition, particularly at pier-foundation junction, the most vulnerable part has been predicted and envisaged, as specified in the article [14]. The recommendations help to provide an outline that an increased stiffness of the pier could possibly be utilized in such a way in withstanding dynamic events in an improved manner. Coupler sections consisting of higher stiffness's are scrutinized as a means of increasing resilience of the ABC pier by manifesting enhanced performance at seismic event to overcome plastic hinge formation at the highly expected vulnerable zones [15]. As such, failure mechanism of individual connector necessitates scrupulous examination before recommending it for widespread use [16]. The present study is an attempt to scrutinize depiction of the individual connector in a connector-system inserted in a foundation for examining the apportioned axial and transversal loads transmitted through main reinforcing steel bar. In short, this study aims to discuss the followings:

- Impact behavior along with serviceability criterion of the connectors placed within the foundation of ABC bridge pier at semi-trailer crash has been scrutinized using analytical method through introducing DIF corresponding to reinforcing steel bar.
- To ascertain the impact behavior, numerical analyses have been intensely taken place through finite element analyses (FEA).
- Manufacturer's supplied material data were utilized to conform the FE model, and experimental testing results were utilized to validate the model.
- Investigation of material resilience of connectors behaving as a composite and their endurance level at high velocity dynamic impact warrants accurate calibration before its widespread practical implementation.

2. Specimen's geometry

A splice-sleeve and grouted coupler data extracted from manufacturer's data has been extracted. As specified, connectors are embedded in a foundation cap. The specific sleeve has been investigated for # 8 ASTM 706 steel bar used as main (longitudinal) reinforcement as specified. By using high strength grout, the steel bars are embedded and aligned in place within coupler. Details of prototyped pier geometries and reinforcements are shown in **Figure 1**.

The reinforcement is aligned in such a way to hold in position by high strength grout. Reinforcing steel bars passing all the through pier has been disconnected within connector to dissipate energy as a post impact phenomenon. The prototyped half-sized representative RC pier has been designed in such a way to utilize a recommended characteristic compressive concrete strength of 3 ksi. The main reinforcing steel bar comprises of grade 60 steel (60 ksi yield strength) and has been designed as recommended by [17,18]. Grade 36 steel (36 ksi) has been considered to be used for

shear reinforcement (transverse), forming helix as shown in **Figure 1**. Sectional elevation and detailed cross-section (c/sec) of the representative pier are also shown in **Figure 1**.

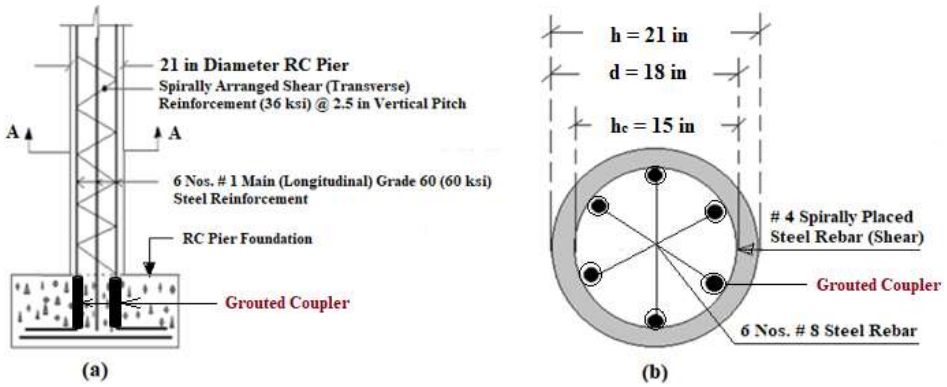

Figure 1. (a) Connector position in the representative pier; **(b)** section A-A.

The pier specimen length is considered as 8.5 feet with a circular c/sec throughout the length. Main reinforcement of six (6) numbers # 8 steel bars all the way to the pier length, followed by a spirally placed transverse reinforcement comprising of # 4 steel (36 ksi) bar @ 2.5 inches (62.50 mm) pitches throughout are kept in the pier specimen. Transverse reinforcement due to withstanding shear limit in a pier specimen provided conforms to the minimum reinforcing shear bar criteria in terms of diameter and pitch as specified in ACI 2011 [19].

3. Methodology

High strain rate dynamic loading incurred from high velocity semi-trailer crash has been considered to investigate for the performance of connectors. The impact performance of the half-sized prototyped representative ABC pier with specified reinforcing steel strength has been utilized as recommended to precisely evaluate deformation at the coupler-steel bar region along with recommended concrete strength while experiencing vehicle hit [8]. The impact subject to concrete strength has been considered as a primary criteria due to its exposed surface is susceptible to car crashes. The impact as primarily experienced by concrete can result significant damage. However, in short, this present study quantifies the distress behavior of the connector embedded at concrete foundation receiving impact from high velocity semi-trailer.

To keep connectors at position, connectors are placed as shown in **Figure 1**. Post impact behavior load transmittance via predicting material properties of the connector is determined by apportioning the load as modelled. The post impact coupler performance has been investigated by carrying out FEA. Material properties are collected from manufacturer's data and used to carry out simulations. Short duration impact performances are considered to examine failure patterns through conducting static and dynamic numerical simulations via FEA. The results captured from FEA has been validated with experimental data to determine DIF's. The respective simulations are conducted by using ANSYS WORKBENCH. The respective DIFs's determined from FEA and damage index (DI) method are correlated followed by validating with the results published in the research article [8]. The results are further

corroborated by carrying out the reliability analysis by estimating reliability index (β).

Properties of connector

Connectors using sleeve and grout as a composite section have been investigated using standardized geometries and material properties as shown in **Figure 1** [20,21]. To put together the precast components of the connector in place needs special detail to behave as a composite section. This type of connection is expected to predict improved performance to withstand short duration, high strain rate dynamic load exerted by high velocity vehicular impact.

Geometrical details of coupler have been considered in this study followed by the standardized specification as recommended. The typically used in ABC connector specified as sleeve number 8U-X that has been shown in the **Figure 2** and **Table 1**. 'Rebar Stop' is shown within the sleeve where reinforcing steel bar has been discontinued. Splice-sleeves made up of cast iron has been used for grouted coupler composite inserted within in the pier along with reinforcing steel bar is embedded, placed, and aligned as shown in **Figure 2**. This arrangement has been made to predict enhanced performance in dynamic response via energy dissipation [12]. The sleeve is filled up by high strength cement grout to hold the steel bar in place with a discontinuation at 'Rebar Stop' as shown in **Figure 2**.

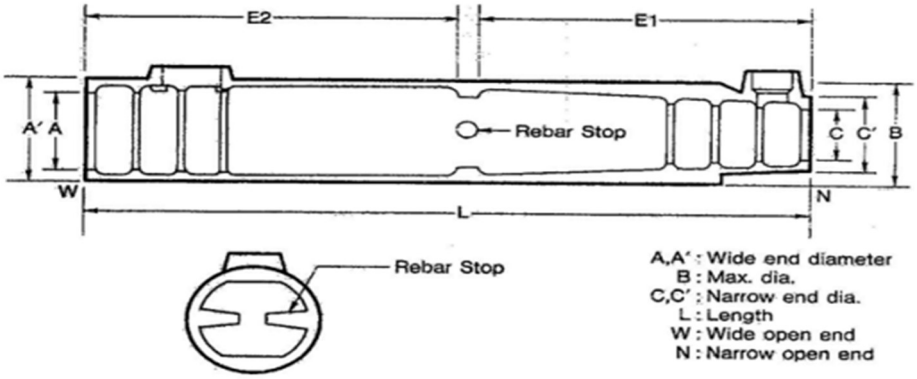

Figure 2. Details of connector [20].

Table 1. Geometry of sleeve number 8U-X [21].

Sleeve zone	Sleeve type	Internal dia. (inch) (mm)	External dia. (inch) (mm)
W = Larger end	8U-X	1.89 (48.01)	2.52 (64.01)
N = Smaller end	8U-X	1.3 (33.02)	2.52 (64.01)

To determine the post impact performance and ascertain the expected plastic deformation, connectors are inserted in stratagem in the region where high stress zones are expected to be formed due to impacting force incurred by high velocity vehicle crash. In addition, with the placing of connector into the foundation has been recommended and as followed by [14]. The connector (grouted coupler) is positioned within the pier section as described in **Figure 1**. Sleeve data has been extracted from manufacturers catalogue has been described in **Table 1** and is as shown in **Figure 3**. Boundary conditions of the prototyped per specimen has been modeled as the upper

and lower ends are restricted from rotation and deflection while upper end is positioned under the axial compression as shown in **Figure 3**. The impact point of pier specimen has been taken at 3 feet (0.914 m) from the foundation top as also shown in **Figure 3**.

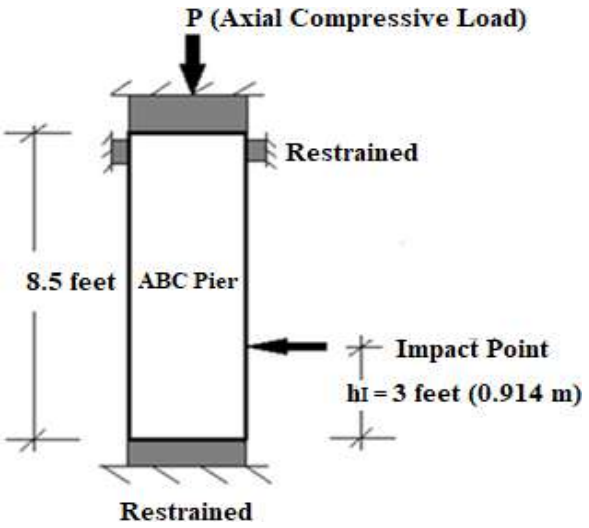

Figure 3. Impact location and boundary conditions.

4. Post-crash behavior of representative bridge pier at dynamic load

Present study investigates that the high velocity impact damage of connector placed within the ABC pier by vehicular. This type of collisions and formation of localized damage along with concrete spalling has been a significant trend. Frequency of occurrence of vehicular crash causing damage seems surpassing the other high strain rate loads like earthquakes and blasts [16]. Furthermore, this can trigger not only deterioration of the pier from cosmetic to collapse but involves overall infrastructural degradation as stated in different studies [22]. High velocity impact from larger vehicles and its severity has received adequate attention. However, specific performance of connectors at high velocity impact experienced from semi-trailer has not yet been fully examined. The connector and steel bar junction region are expected to evince pertinent stress limit over the stress resulted by impact for ensuring serviceability criteria. Expected plastic hinge is likely to be formed at 150% of the yield strength as specified of inserted reinforcing steel bar as recommended by [15]. Stresses are estimated using FEM to examine the connector and steel bar at post performances. The mobile dislocating velocity increases at a higher rate to accommodate the required plasticity has already been discussed [22]. Results captured from post deformed models are considered for analyzing performance behavior. This leads to accomplish rate sensitivity analyses through high stresses induced resulting large deformation taken place.

4.1. Flexural properties of connector

Flexural properties have been determined from withstanding axially compression static load (P_n) of the specimen and shall be determined by using Equation (1).

$$P_n = 0.85 \times f_c'\left(A_g - A_s\right) + A_s f_y \quad (1)$$

where: A_g and A_s indicate c/sec areas of pier and the area of longitudinal steel, and f'_c and f_y conforms the concrete strength in compression at 28 days and reinforcing steel bar in tension.

Post impact performances of the coupler model hit by fractioned transmitted has been studied for flexure and shear. Determination of transmitted loads passing through the longitudinal axis of column specimen and via respective main reinforcing steel bar are included in respective **Tables 1** and **2**. The evaluated results comprising axial compressive force carried out by the pier specimen has been shown in **Table 2**.

Table 2. Pier geometry and material properties.

f'_c (ksi) (MPa)	f_y (ksi)(MPa)	A_g (in^2) (mm^2)	A_s (in^2) (cm^2)	P_n (kips) (kN)
3 (20.68)	60 (413.68)	346.50 (2235.48)	4.70 (30.32)	1310 (5827.17)

Apportioned axial load transmitted by the column specimen has been incurred by each connector pier has been evaluated via each elements considering a composite sectional phenomenon. Axial compression governed by each connector conforming material properties and geometries obtained from the literature can be determined through Equation (2).

$$P_{n,s} = (P_n) \times \left[\frac{A_{CI} \times E_{CI} + A_{Grout} \times E_{Grout}}{A_{net} \times E_{Concrete} + A_s \times E_s}\right] \times \eta \quad (2)$$

where: P_n and $P_{n,s}$ express the design axial loads (compression) of the specimen and fractioned each reinforcing steel bar respectively; A_{CI}, A_s, and A_{Grout} express overall cross-sectional area (c/sec) of cast iron component of the splice sleeve, c/sec area of main reinforcement, and c/sec area of filled and compacted grout; E_{CI}, E_{Grout}, $E_{Concrete}$, and E_s indicate respective material moduli of the hollow splice sleeve made up with cast iron, high strength grout, peripheral concrete, and main reinforcing steel bar; and η is the energy dissipation factor. To analyze the coupler behavior, $E_{Concrete}$ is considered as 2.65 psi, and the respective values of E_{CI}, E_{Grout}, and E_s are considered.

The apportioned axial compressive force transmitted into each connector has been evaluated by Equation (2) yielding 3.01 kips (13.38 kN).

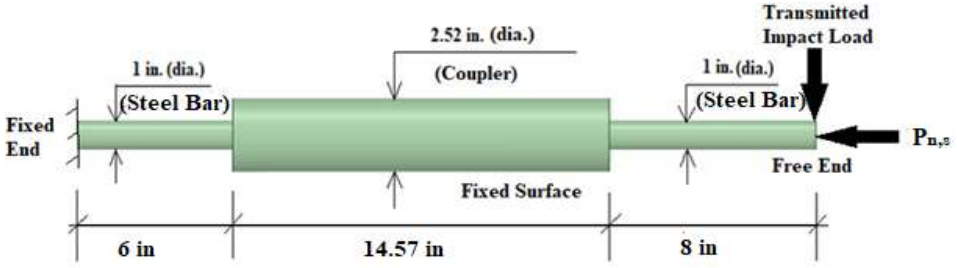

Figure 4. Load model of coupler and main steel bar.

$A_{connector}$ indicates the simple scaler addition of hollow cylindrical splice sleeve (cast iron) c/sec and c/sec of high strength cement grout. From geometry, $A_{connector}$ can be deduced by summing up A_{CI} and A_{Grout} using **Figures 4** and **5** and is shown in Equation (3).

$$A_{connector} = A_{CI} + A_{Grout} \tag{3}$$

where: $A_{connector}$ is the gross c/sec area of connector filled up with high strength cement grout; and A_{CI} and A_{Grout} are already explained as shown in **Table 3**.

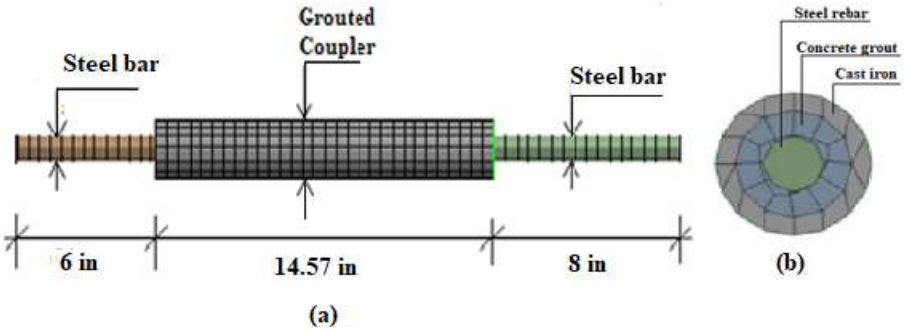

Figure 5. Mesh of grouted coupler for **(a)** longitudinal view; **(b)** top view.

Using **Table 1**, and **Figures 4** and **5**, $A_{coupler}$ can be evaluated as 2.20 in^2 (14.20 cm^2).

The transmittance of impact force into pier specimen under axially transferred preload and the inter-materialistic interaction of the composite connector needs an insight to inspect the complex mechanism during and after high strain rate vehicle crash. However, initially shear force administers the post impact behavior and is followed by the force due to flexure which brings about an intricate phenomenon. Axial force being a secondary controlling factor for which the vehicle crash is governed, an imperceptible amount of apportioned axially compressive force (η is approximately considered as 0.2% due to energy dissipation effect) has been transmitted to the connector composite after being dissipated a considerable amount of energy. To alleviate the effect of modulus of individual composite material in controlling the impact mechanism, Equation (2) has been simplified and approximated. This results a close proximity following same outcome within a minimal of 2.9% variation can be precisely estimated by using Equation (4).

$$P_{n,s} = P_n \times \left[\frac{A_{connector}}{A_{net}}\right] \tag{4}$$

where: P_n, $P_{n,s}$ and $A_{connector}$ are already explained; A_{net} expresses net c/sec area of the connector.

The fractioned design loads resulted from Equation (1) through Equation (4) are given in **Table 3**.

Table 3. Design values of respective axial loads.

P_n (kips) (kN)	$P_{n,d}$ (kips) (kN)	$P_{n,s}$ (kips) (kN)
1308.20 (5819.16)	1310 (5827.17)	3.01 (13.38)

4.2. Estimation of DIFs

The DIFs in reinforcing steel (dynamic increase factor) has been evaluated by the ratio of the dynamic over static counterpart forces incurred by high strain rate loading of the specific element as recommended [23]. Longitudinal steel bar used as main

reinforcement in the pier being considered as an isotropic and homogeneous material can be most likely to dissipate higher percentage of energy and carries out relevant amount of impact load. Determination of DIF for main reinforcing steel bar needs to be essentially evaluated the static counterpart of shock exerted by high velocity semi-trailer crash. This has been put together and shown in **Table 4**.

Table 4. Determination of dynamic coupler moment.

I_S (kips) (kN)	h' (feet) (m)	M_s (kip-ft) (kN-m)	DIF	M_{dyn} (kip-ft) (kN-m)
3271.89 (14,554.12)	3 (0.91)	22.26 (30.16)	1.053	23.44 (31.78)

Impacting vehicular weight (W) along with the crashing velocity (V) of the semi-trailer are considered as 42.11 kips (187.30 kN) and 100 ft/s (30.48 m/s) respectively conforming standardized specifications. Permissible vehicular speed has been considered as recommended in the standardized specification [24]. Determination of DIF as a pertinent criterion of vehicular impact needs to be evaluated. Dynamic flow stress (σ_{dyn}) of main reinforcement during high strain rate vehicle crash has been estimated by using Equation (5), as recommended by [3].

$$\sigma_{dyn} = (\sigma_y) \times \left[1 + \left(\frac{\dot{\varepsilon}}{C}\right)^{1/p}\right] \tag{5}$$

where: σ_y is a static flow stress of for ASTM A 706 (ASTM 2015) using Grade 60 steel bar and is considered as 60 ksi (420 MPa); C addresses as material coefficient and p indicates the strain rate parameters which are considered as 40 and 5 respectively [9]. Rate of change of strain with the time of main reinforcing steel bar ($\dot{\varepsilon}$) has been utilized as 0.16 s^{-1} for specific vehicle crashing high velocity speed at 100 ft/s (30.48 mtr/s). Severity of damage level during high-speed vehicle collision considering non-linear trend of transverse loading incurred from horizontal impact has been estimated [25]. Using Equation (5), σ_{dyn} (Dynamic flow stress) has been determined that yields the result as 79.80 ksi (550.2016 MPa).

Using Equations (3) through 5, the dynamic parameter 'ψ' can be determined by utilizing the Equation (6) as recommended by [26,27].

$$\psi = 0.019 - (0.009) \times \left[\frac{\sigma_{dyn}}{60}\right] \tag{6}$$

where: ψ is termed as dynamic parameter which is a function of yield stress at the strain hardening zone, and σ_{dyn} is the dynamic flow stress at uniaxial plastic strain rate of steel.

Equations (6) results ψ as 0.0172 after inserting σ_{dyn} using Equation (4) as 79.80 ksi.

Dynamic Impact factor of the main reinforcement (DIFs) can be estimated from Equation (7) by using ψ correspondingly evaluated from Equation (7) [27].

$$\text{DIFs} = \left(\frac{\dot{\varepsilon}}{10^{-4}}\right)^{\psi} \tag{7}$$

where: DIFs and ψ are already explained; and $\dot{\varepsilon}$ expresses as strain rate of main

reinforcing steel.

Analytical estimation of DIF using Equation (7) has been evaluated as 1.053.

4.3. Computation of analytical static and dynamic forces of coupler

Static impact force (I_S) due to vehicular collision can be estimated by using Equation (8).

$$I_S = \frac{W \times V}{\tau} \tag{8}$$

where: I_S addresses impact force at static condition, W indicates the weight of semi-trailer (42.11 kips or 19099.87 kg-wt); V is expressed as the maximum permissible crashing speed being considered as 100 ft/s (30.48 m/s) [3], τ is crashing time from impact till post impact deformation being considered as 40 ms (milli-second) [3], and h_I has been considered as the height of impact as shown in **Figure 3**.

Inserting the values in Equation (8), yields I_S as 105270 kip-ft/s^2 or 142,114.50 kN-m/s^2 (corresponding equivalent load is 3271.896 kips or 14,554.12 kN) [28,29].

Pier experiencing equivalent static moment (M_s) can be estimated from Equation (9) using I_s and h_I.

$$M_S = I_S \times h_I \tag{9}$$

where: I_s and h_I have already been expressed.

Approximated load apportioning has been executed in a simplified way after multiplying M_s as shown in Equation (8) with area ratio expressed as $A_{\text{connector}}/A_{\text{net}}$. This leads to estimating the static moment incurred by a single connector ($M_{s,c}$) as furnished in Equation (10).

$$M_{s,c} = M_s \times \left[\frac{A_{connector}}{A_{net}}\right] \tag{10}$$

The corresponding dynamic moment exerted by single connector ($M_{dyn,c}$) can be estimated via DIF multiplied with $M_{s,c}$ as shown in Equation (11).

$$M_{dyn,c} = \text{DIF} \times M_{s,c} \tag{11}$$

where: $M_{s,c}$, $M_{dyn,c}$, and DIFs are already addressed.

Equation (10) yields $M_{s,c}$ as 22.26 kip-ft (30.17 kN-mtr). The corresponding $M_{dyn,c}$ has been determined by Equation (11), resulting as 23.44 kip-ft, (30.18 kN-mtr). The resulting moments at connector and steel bar junction are as shown in **Table 4**. As the dynamic properties cannot be estimated directly due to short duration collision strike, it can be indirectly determined by using the DIFs [10]. Semi-trailer vehicle weight [30] has been considered for evaluating impact force and utilized from the data given and as shown in **Table 4**.

The apportioned loads transmitted to the single coupler composite via reinforcing steel of the connector system has been determined for axial compression ($P_{n,s}$) evaluated as 3.01 kips (13.40 kN) that has been already discussed in Section 3.1. The fractioned transverse load as modelled at the free end of individual reinforcing steel bar (longer edge as shown in **Figure 4**) are developed from the static moment (M_s) as a result of the vehicle crash, which additionally incurs moment at connector and steel bar junction comprising of conservative analyses. Using Equation (10), M_s has been

evaluated as 22.26 kip-ft. (31.54 kN-m) which results high stress in the coupler-steel bar junction depicting large deformation for both static and dynamic analyses. Energy dissipation is expected to be taken place considerably during and immediate after the impact expecting large plastic deformation to be occurred as the stiffness's of the members warranting flexural resilience being reached at elastic-plastic state [30].

5. Numerical modeling (FEM) of grouted coupler

Numerical simulations are conducted by using FEM which has been used to assess the individual connector performance. Commercially available 'ANSYS' has been extensively used to evaluate static and explicit dynamic performances. To develop the FE model, hollow cylindrical cast iron splice-sleeve conforming strength of 36 ksi (248 MPa) is used along with 6 ksi (41.36 MPa) cement grouting and # 8 reinforcing steel bar embedded into the grout, as shown in **Figure 2**. For all different material's connections, composite coupler system has been considered for developing the FE model. The mesh size considered for the simulations by going through mesh-independence studies and is considered as 0.01 in. (0.254 mm). Reinforcing steel bar conforms specified yield strength (60 ksi or 420 MPa) are embedded and extended from coupler in both sides are 8 in. (20.32 cm) and 6 in. (15.24 cm) respectively, as shown in **Figure 4**. The external peripheral surface of the splice-sleeve is considered as fixed as it is embedded and placed within the foundation concrete. The free end of the 6 in. side is also considered as fixed (as shown in **Figure 4**) as it is extended within the foundation receiving adequate development length.

FEA models are generated in such a way where the apportioned axially compressive load and moments are transmitted via incorporating area ratio described as ($A_{coupler}/A_{net}$). To compare and validate the DIF's computed from FEM and the analytical formulations, stress ratio ($\sigma_{dyn}/\sigma_{static}$) is considered via using έ as shown in Equation (4). Apportioned horizontal (shear due to impact) and axial (flexure due to axial bending) forces are exerted on the model from the respective forces force of pier deployed at the free end (8 in. edge of steel bar from pier base and foundation top within pier) and is shown in the **Tables 3** and **4**. Boundary conditions of the FE model are elaborately furnished in **Figure 4**.

Table 5. Manufacturers supplied material properties [15].

SL. No.	Properties	Cast iron	Grout	Steel bar
1	Density (pci) (kN/m^3)	0.284 (77)	0.083 (22.53)	0.284 (77)
2	Modulus of Elasticity (psi) (MPa)	29×10^6 (2×10^5)	43.51 (0.3)	29×10^6 (2×10^5)
3	Poisson's ratio	0.3	0.3	0.3
4	Bulk modulus (psi) (MPa)	2.42×10^7 (1.6×10^5)	2.26×10^6 (1.6×10^4)	2.42×10^7 (1.6×10^5)
5	Shear modulus (psi) (MPa)	1.12×10^7 (7.7×10^4)	1.84×10^6 (1.26×10^4)	1.12×10^7 (7.7×10^4)
6	Tensile yield strength (psi) (MPa)	3.62×10^4 (249.6)	0	3.62×10^4 (249.6)
7	Tensile ultimate strength (psi) (MPa)	3.62×10^4 (249.6)	0	6.67×10^4 (459.8)
8	Compressive ultimate strength (psi) (MPa)	0	5.95×10^3 (41.02)	0

Material properties are extracted from manufacturer's (NMB Splice Sleeve Inc., North America) data to develop composite FE model. Using this, FE model has been

developed to carry out simulations under high velocity vehicle impact. In addition, **Table 5** illustrates the manufacturer's supplied material properties that have been collected and utilized to develop FEM.

5.1. Connector composite meshing system

The connector along with the embedded reinforcing bars are meshed for the analyses and is considered as 0.01 in. as shown in **Figure 5**. All elements conforming square mesh has been considered. Mesh sizes are further reiterated from 0.1 in., and 0.05 in. respectively to carry out the sensitivity analyses showing if any variation in the results can be apprehended. For all three different materials, a composite system has been modelled to be incorporated and acting as a monolithic composite behavior under the specific load as shown in **Figure 4**. However, **Figure 5** shows FE model represents mesh independence with its size converges at 0.01 in^2 (0.254 mm^2).

5.2. Mesh sensitivity (refinement) study of FEM

Mesh independence studies are performed for respective mesh sizes of 0.1 in., 0.05 in. and 0.01 in, where results from Von-mises stress, strain and total deformation are considered. Simulations are carried out for both static and dynamic impacts. Different mesh sizes are considered for examining mesh convergence and thus the optimization via mesh refinement has been obtained. Mesh sizes utilized for pursuing the simulations show the results are within permissible range. To conduct static and explicit dynamics analyses, mesh sizes are conformed to 0.01 in^2 (0.254 mm^2) through performing sensitivity analysis. Results captured from static and explicit dynamic are plotted in **Figures 6–8** respectively considering mesh sizes comprising deformation and strain. Static analyses show the linear trends while dynamic analyses contemplate non-linear trends to come up with the optimal mesh size.

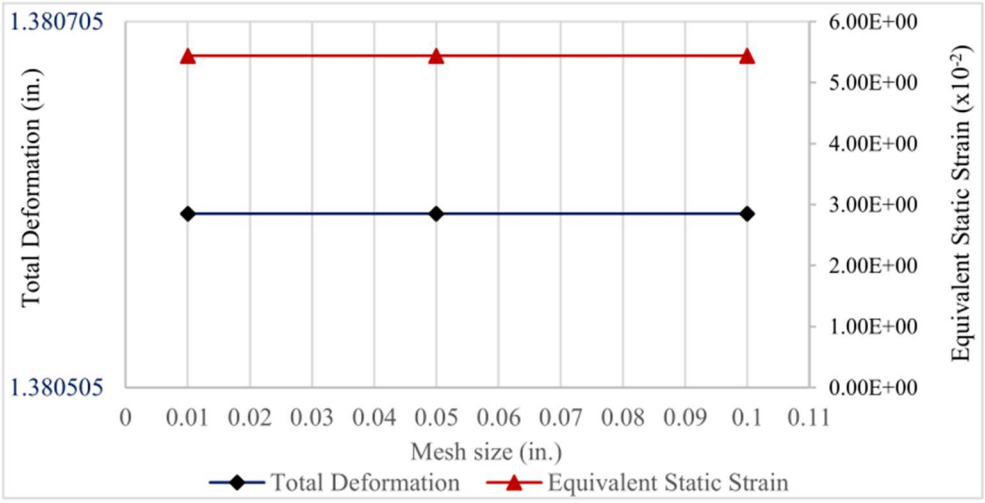

Figure 6. Results for mesh independence for static deformation and strain.

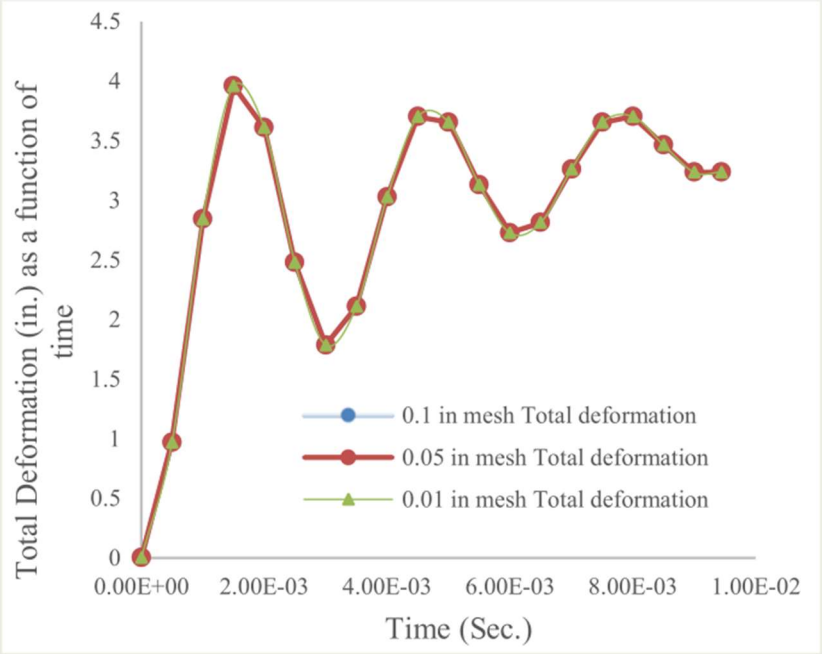

Figure 7. Dynamic mesh independent results for deformation.

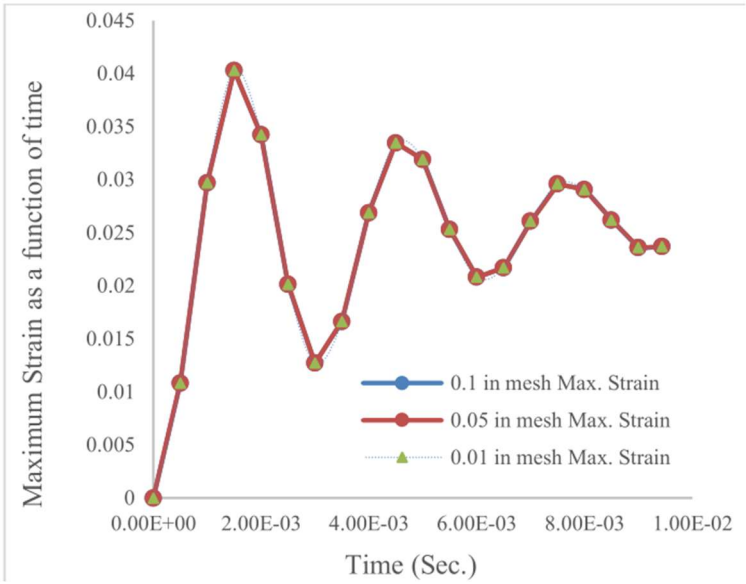

Figure 8. Dynamic mesh independent results for maximum strain.

5.3. Uncertainty assessment using confidence interval (CI)

Confidence Interval (CI) has been utilized to capture the degree of uncertainty for assessing the numerical results evaluated from dynamic simulation using normal distribution. CI is also able to evaluate the probability that a parameter falls between a pair of values around the mean. Thus, the confidence interval (CI) is utilized to assess uncertainty, and determined via using mean (μ), standard deviation (SD), confidence level (z) and sample size (N) (as shown in **Table 5**), and is as shown in the Equation (12). CI helps provide to assess the role of uncertainty parameters during car crashes.

$$\mathrm{CI} = \mu \pm z \times \left[\frac{SD}{\sqrt{N}}\right] \tag{12}$$

where: μ is the mean of sample size, SD is the standard deviation, N is the sample size considered as one thousand data, and z is the confidence or significance level considered as 98%.

CI data to capture the uncertainty is shown in **Table 6**.

Table 6. Input data for CI.

Input variables	σ_D (psi)	εD	E_D (psi)
Significance Level (z)	0.02	0.02	0.02
Mean (μ)	668,798.4	0.023975	32,417,194
Standard Deviation (SD)	628,000	0.008989	628,000
Sample size (N)	1000	1000	1000

5.4. Reliability analysis

Monte Carlo simulations being expensive and requiring millions of simulations, moment-based methods such as the Hasofer-Lind reliability index (β) method is one of these methods that was developed as an alternative to the simulations and has been recognized as an effective and precise method to estimate structural safety. This method is considered in this study for its advantage over other moment-based methods including its invariance to the specific form and not requiring prior knowledge of the distributions of the variables.

5.4.1. Integrity analysis

To estimate β via integrity analyses using factor of safety (F) from using results extracted from FE results as shown in **Table 4**, Equation (13) can be fairly used [31,32]. The Hasofer-Lind reliability index [33] is computed using an iterative procedure involving reduced variates, using factor of Safety (F) from the materials integrity, capturing data from FEA and variables as computed in [34,35].

$$\beta = \frac{E(F) - 1}{SD \times (F)} \tag{13}$$

where: β is the reliability index, F (moduli of dynamic over static using numerical simulation) is the factor of safety computed from dynamic simulation results, E is the modulus of elasticity and SD is the standard deviation.

5.4.2. Direct reliability index

Performance reliability (β) of the individual coupler is further determined directly by using the probability of failures (P_f) resulted from dynamic simulation [32]. Results from the dynamic analysis is utilized as modulus of maximum elasticity (E) in demand utilizing dynamic DIF resulted from simulation (shown in Equation (10), E as 30×10^6 psi), as it exceeds the material E-modulus (29×10^6 psi). Maximum resulted stresses and strains from dynamic numerical simulations in terms of E-modulus in demand due to post impact behavior are captured to evaluate dynamic amplification effect (DIF) as 1.07 through the ratio of dynamic moduli (dynamic modulus/static modulus) draw an insightful correlation between DIF's computed analytically as 1.053. This result triggers to evaluate failures and corresponding reliabilities of coupler. Performance reliability (β) of the individual coupler can also be computed directly

from probability of failure (P_f) is evaluated from the DIF's with a difference of 1.6% which results as 0.0021 by using the inverse of the standard normal cumulative distribution functions of probability of failures (P_f) resulted from direct approximation method and is as shown in Equation (14) [33].

$$\beta = -\Phi^{-1}(P_f) \tag{14}$$

where: P_f is the probability of failure and Φ^{-1} is the inverse of the standard normal cumulative distribution function.

6. Results

6.1. Results using FEM

Results captured from using FE models shows substantial deformations along with high stress and strain are also observed. Large deformation at the free end of bar where loads are applied depicts failure occurring at the junction of steel bar and connector.

6.1.1. Static analysis

Results from static analysis present considerable deformation at the main reinforcing steel bar. Deformations in both *X* and *Y* directions seem uniform, as 0.12 in. (0.004 mm.) and as shown in **Figure 8**. High strain concentrations and significant stress are observed in the contact of grouted coupler and steel bar as shown in **Figure 9** through 11. Maximum permissible material modulus instilling material modulus (Maximum stress/Maximum strain) requirements are observed from the simulation results subjected to static strain yields as 1.38 (as shown in **Figure 10**) and static stress (as shown in **Figure 11**) comprises 8.51×10^5 psi (5.8×10^3 MPa). The deformations are observed in both the directions and estimated as 1.375 in. (34.925 mm) and 0.12 in. (3.02 mm) for static (**Figure 12**), and 2.38 in. (60.45 mm) and 0.11 in. (2.80 mm). The material modulus in demands depict as 6.17×10^5 psi (7.57×10^5 MPa) for steel bar at the coupler junction. This endorses material property can be safe enough as modulus of elasticity incorporating reinforcing steel bar has been commonly considered as 29×10^6 psi.

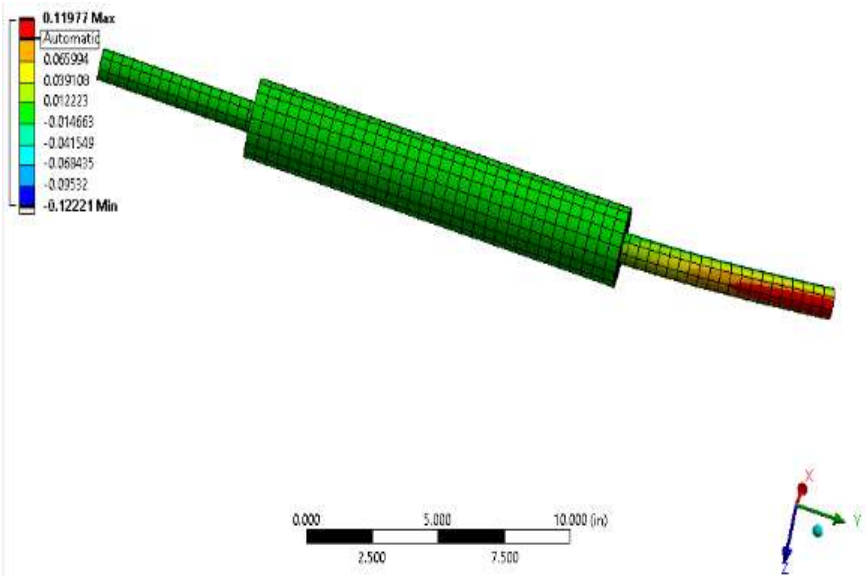

Figure 9. Directional deformation.

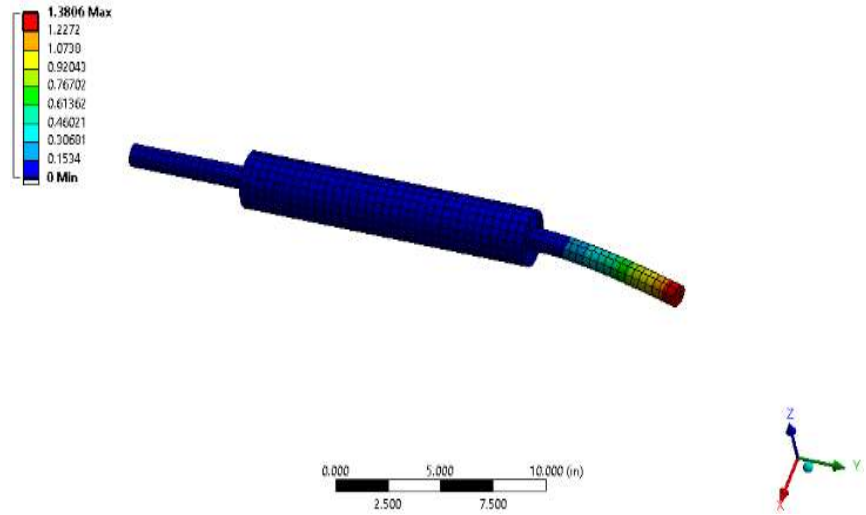

Figure 10. Static strain.

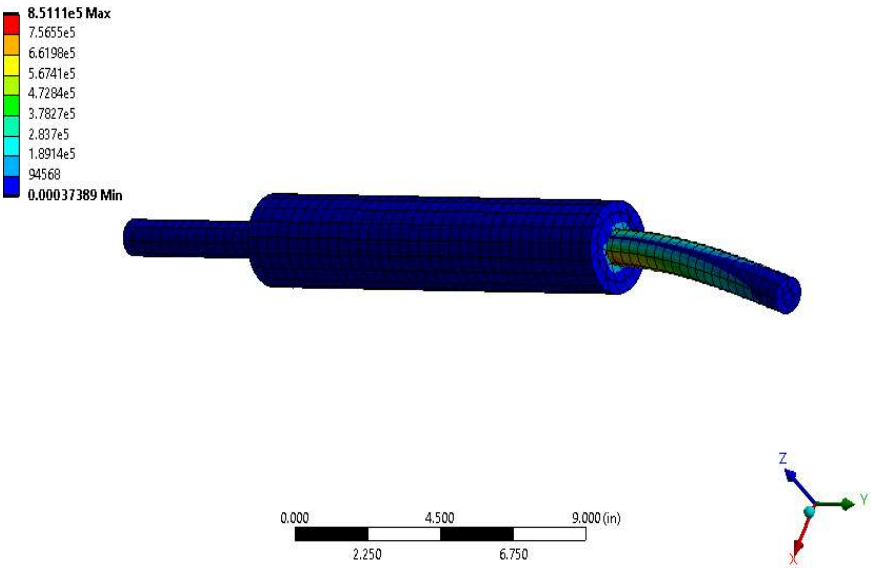

Figure 11. Static stress.

Dynamic results incorporating time-dependent studies are shown in **Figure 12**. This also observes directional deformations and provide quite different results in the respective directions (3.15 in. and 0.12 in.) along *X* and *Y* as shown in **Figure 12a,b** respectively with tight R^2 values of 0.999 and 0.996 which conform optimistic trend of static strain and stress.

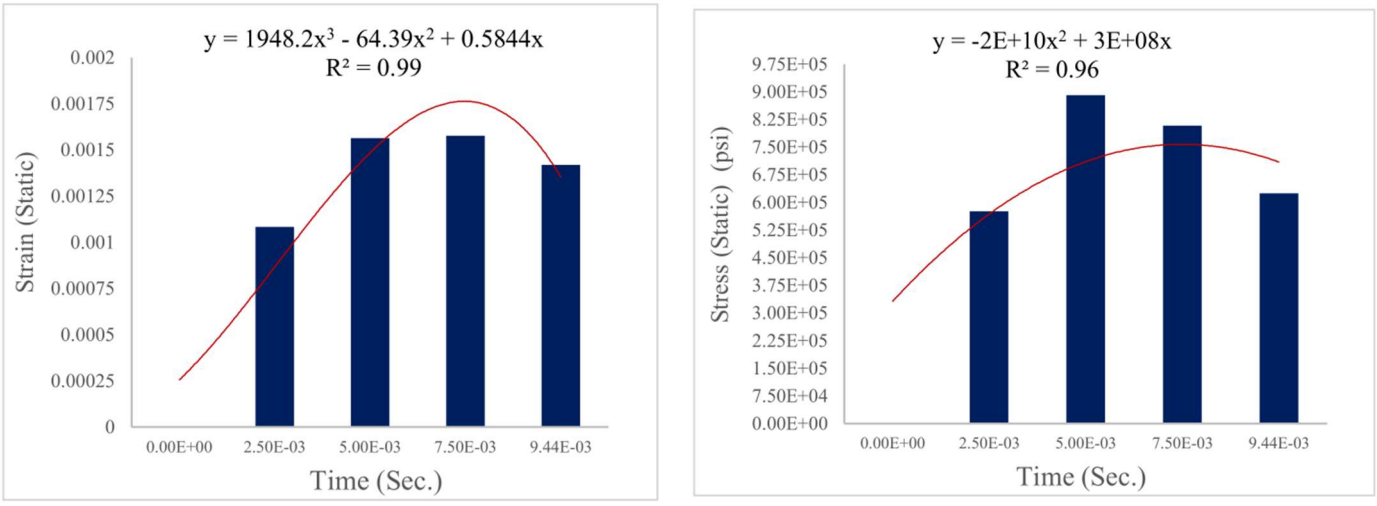

(a) **(b)**

Figure 12. (a) Time-dependent static strain; **(b)** time-dependent static stress.

6.1.2. Dynamic analysis

Results from explicit dynamic analyses show significant deformation at steel bar as high stress and strain have resulted at the junction as shown in **Figures 13–15**. Maximum permissible material modulus (Maximum Dynamic Modulus = Maximum dynamic stress/Max. dynamic strain) at dynamic load requirements from simulations subjected to dynamic stress and strain are 6.25×10^5 psi (1.82×10^5 MPa) and 0.2 which are exceeded by the material E-modulus. Using maximum dynamic stress (**Figure 14**) over dynamic strain, modulus in demand (maximum dynamic stress/maximum dynamic strain) is computed as 31.25×10^6 psi (2.15×10^5 MPa), whereas material E-modulus is commonly considered as 29×10^6 psi (2.1×10^5 MPa). However, demand of material modulus for dynamic over material from FE analysis is computed as 1.07, whereas the numerical DIFs is computed as 1.053. For dynamic analyses, results captured for parallel and perpendicular to the application of load have been shown in **Figure 16**. Time-dependent dynamic strain and stress are captured and are shown in **Figure 16**.

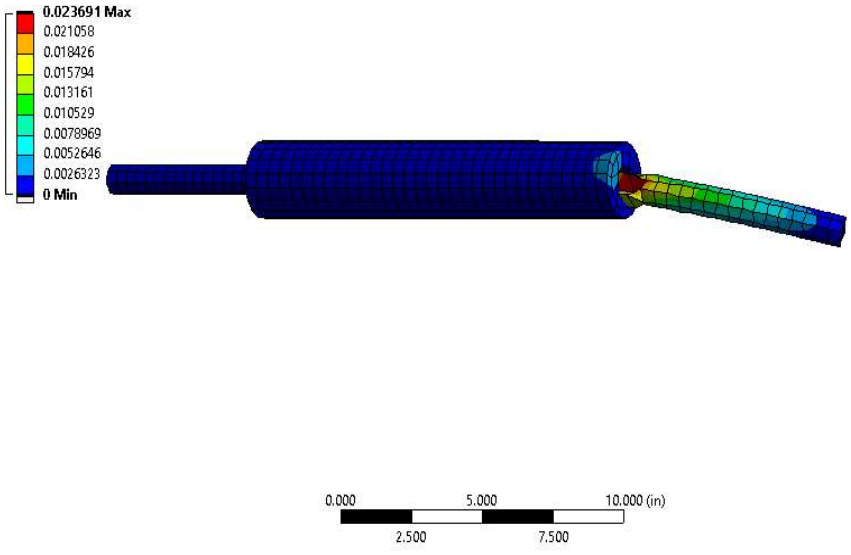

Figure 13. Directional deformation.

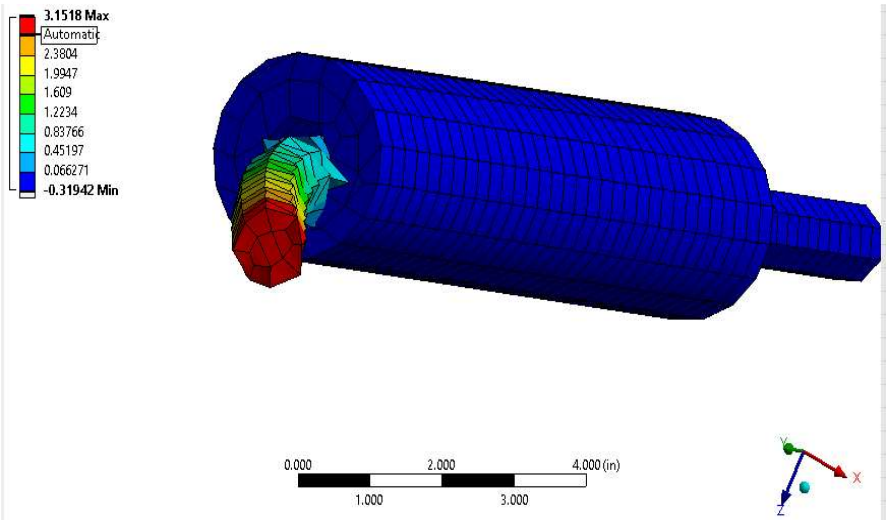

Figure 14. Dynamic strain.

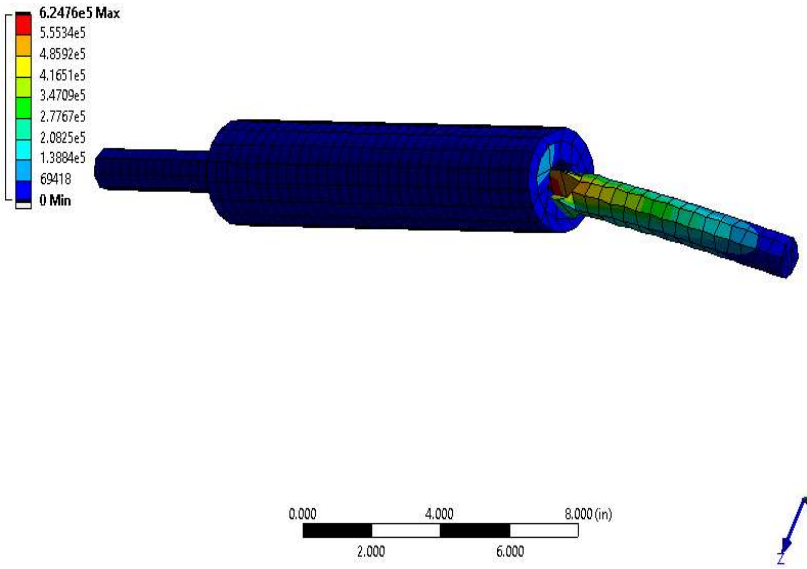

Figure 15. Dynamic stress.

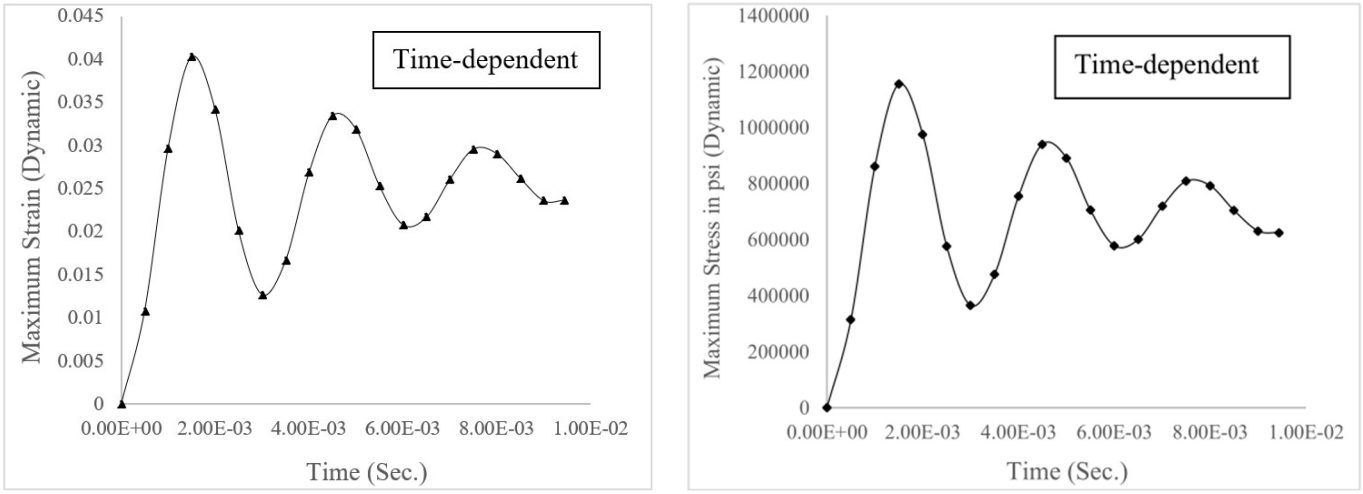

(a) **(b)**

Figure 16. (a) Dynamic strain; **(b)** dynamic stress.

Transmitted dynamic impact load parallel and normal to the external applied loads resulting large deformations are captured are shown respectively in **Figure 17a,b**. Resulted deformation that takes place parallel to the load seems significantly higher than that of the normal. To avoid the discrepancies in capturing deformations at different directions as a function of time, dynamic simulation has been carried out to determine maximum plastic deformation. **Figure 17** shows the deflection behavior at the post impacted distress.

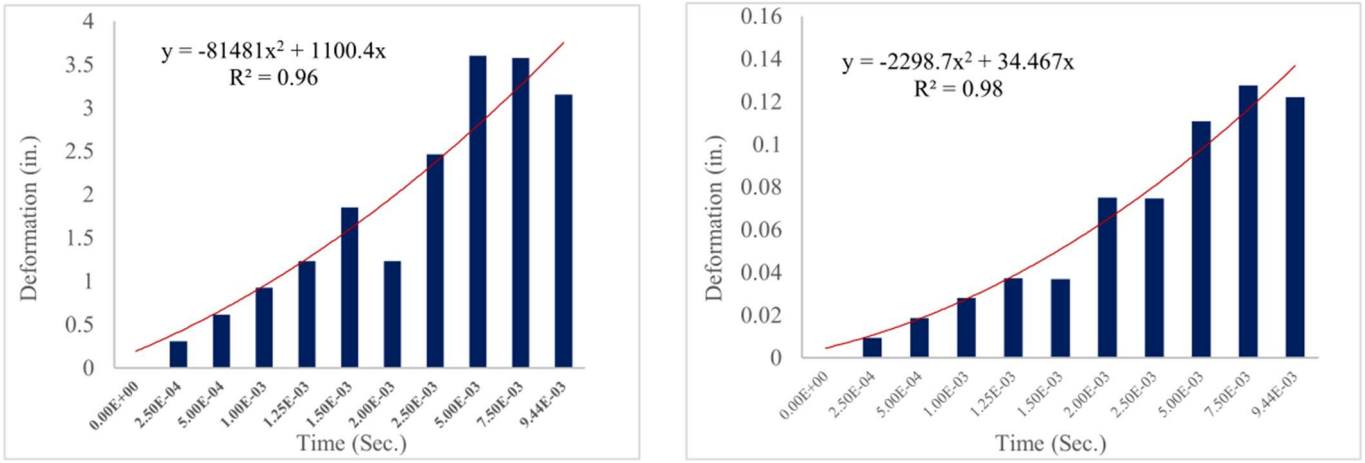

(a) **(b)**

Figure 17. (a) Deformation parallel to load; **(b)** deformation normal to load.

In **Figure 17a,b**, the respective captured deformations from FE simulations confirm the trend patterns are proximately justifiable as the respective R^2 values are shown as 0.96 and 0.98.

6.2. Regression results of dynamic analysis

Resulted stress corresponding to plastic strain captured and plotted from dynamic simulations can well estimate the non-linear trend of material performance via regression analysis. To come up with the non-linear trend via evaluating of

performance function (g), the resulted dynamic stress and strain at plastic zone are plotted as shown in **Figure 18**.

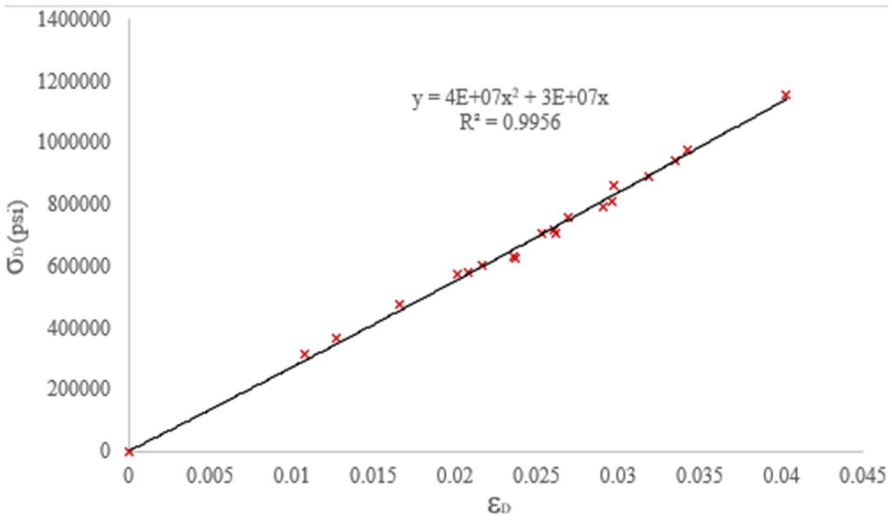

Figure 18. Result of dynamic stress and strain.

As shown in **Figure 18**, regression results are plotted with the observed R^2 yield as 0.99.

$$g(\sigma_D, \varepsilon_D) = \sigma_D - 4.10^7 \times (\sigma_D^2) - 3.10^7 \times (\varepsilon) \quad (15)$$

where: σ_D expresses dynamic stress concentration, ε_D is the dynamic strain, and g is the post impact performance function.

6.3. Model integrity analysis

Anomalies in the results captured from static and dynamic simulations and complexities involved to control material behavior at post impact performance. Exceeding dynamic over static material modulus at plastic zone, and dynamic results for material modulus in demand are governed to carry out integrity analysis of the model. Integrity analysis includes statistical parameters of mean (μ), covariance (V) and standard deviation (SD) resulted from dynamic simulations and is given in **Table 7**. To carry out simulations, one thousand data comprising of dynamic stress and strain were developed by using random variables depicting dynamic stress (σ_D), dynamic strain (ε_D), and material modulus considered between yield to plastic zone (E_D). The computations have been conducted using EXCEL by generating RAND function. This has been inculcated from random variables to run the regression analysis (**Figure 19**). Integrity analysis has been conducted from using the dynamic simulation results utilizing **Table 4**.

Table 7. Variables μ, V and SD.

Variables	μ	V	SD
σ_D	6.74×10^5 psi (4647.06 MPa)	0.383	2.58×10^5 psi (1778.84 MPa)
ε_D	0.024	0.38	0.0091
E_D	2.65×10^5 psi (1827.11 MPa)	0.237	6.28×10^5 psi (4329.91 MPa)

The respective statistical parameters μ, V and SD are utilized for obtaining the respective dynamic parameters σ_D, ε_D and E_D. The dynamic parameters are also extracted from the simulation results executed from the simulated results captured from FE analyses.

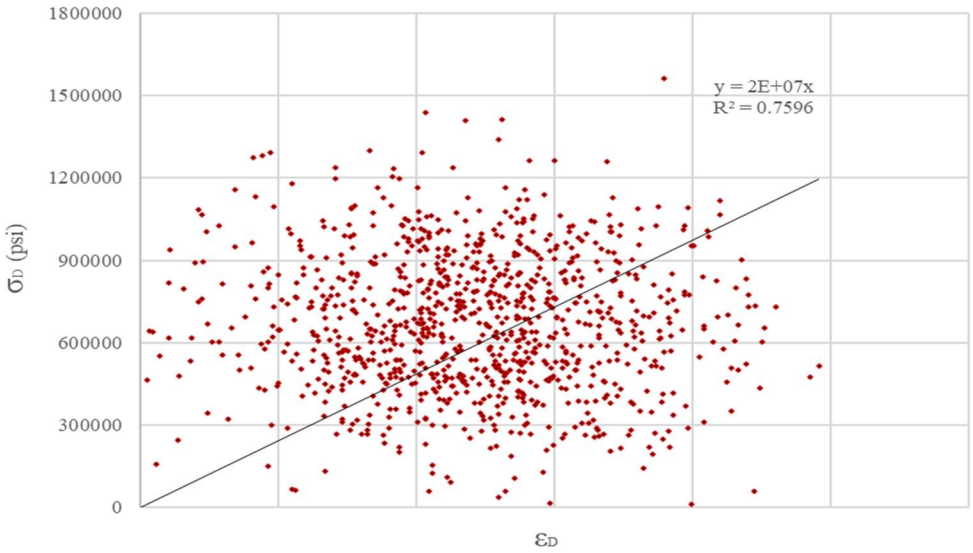

Figure 19. Dynamic stress and strain results using integrity analysis.

With the virtue of regression analysis, results from explicit dynamic undergoing FEA are captured and plotted, and as shown in **Figure 19** in terms of performance function (g) which is given Equation (14). This equation will help to provide higher precision via linearizing results with a relatively flexible R^2 value of 0.76.

$$g(\sigma_D, \varepsilon_D) = \sigma_D - (2 \times 10^7) \times (\sigma_D^2) \quad (16)$$

where: g, σ_D and ε_D are already explained.

6.4. Performance reliability of coupler

The results comprising reliability indices based on vehicle impact performance for RC ABC pier is determined and as shown in **Figure 20**. This study has been carried out using FE model incorporating static and dynamic analyses. Performance of coupler-embedded (ABC) RC pier is determined from the stress developed at coupler using the conservative results from dynamic simulation in experiencing high velocity vehicle impact.

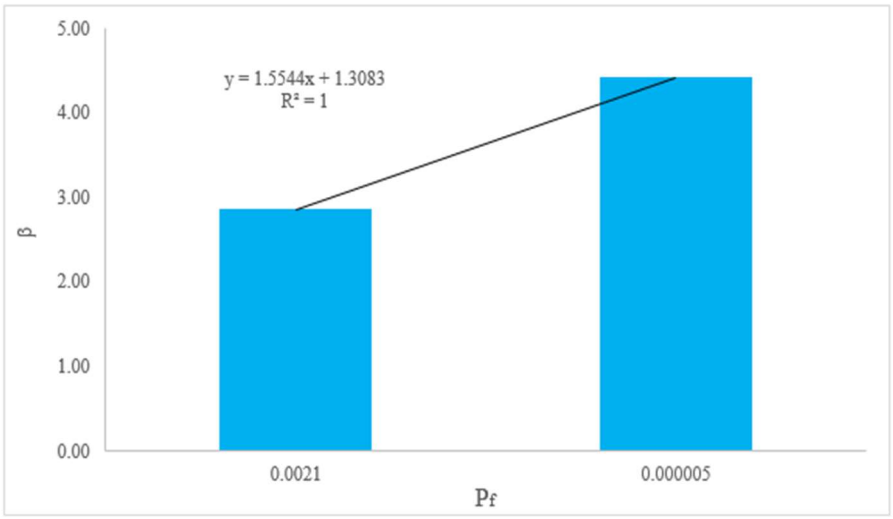

Figure 20. Determination of β from P_f.

6.4.1. Performance reliability using integrity analysis

Using Equation (14) and **Table 4**, β is evaluated from integrity analysis utilizing F results (F as 5.16×10^{-3}) yields 4.4 with a corresponding approximate P_f of 5×10^{-5}.

6.4.2. Performance reliability using direct reliability method

Post impact performance as a reliability index (β) is also directly evaluated from probability of failure (P_f) as a function of DIF. Result from the dynamic analysis is utilized as dynamic modulus of material in demand using DIF resulted from simulation exceeding the material E-modulus. This result leads to evaluate failures and corresponding reliabilities of coupler. The performances are evaluated by determining probability of failures (P_f) and corresponding performance reliability through integrity analyses (IA) from resulting stress and strain from conservative dynamic impact. The IA of the impacted pier is conducted using resulted stresses and strains from FEA. Stresses resulted due to impact and the dynamic amplification effect (DIF) draw an insightful correlation between DIF's computed analytically (1.053) and numerically using the FE simulation (1.07) through the ratio of moduli. Probability of failure (P_f) is evaluated from the DIF's with a difference of 1.6% which results as 0.0021. Performance reliability (β) has been directly computed using Equation (13), yields as 2.86.

6.4.3. Determination of reliability index

Reliability Index (β) of the coupler can be determined using Sec. 3.2.1 and 3.2.2 from the corresponding probability of failures (P_f). The comparative results are put together and is as shown in **Figure 20**.

Using **Figure 20**, overall β of the coupler undergoing high velocity vehicle impact can be determined using the results of the regression analysis with R^2 value of 1 as shown in Equation (14).

$$\beta = 1.6.P_f + 1.31 \tag{17}$$

where: P_f and β are already explained.

6.4.4. Uncertainty assessment using confidence interval (CI)

To ascertain integrity, confidence Interval (CI) has been further utilized to

estimate the degree of uncertainty for assessing non-linear results comprising of σ_D, ε_D, and E_D. The uncertainty in the results has been determined using the CI has been already exhibited in **Table 6** which is, in addition, precisely presented in **Table 8**.

Table 8. CI results.

Variables	Confidence value (CV)	Confidence interval (CI)
σ_D (psi)	46,199.18	$(7.15 \times 10^5, 6.22 \times 10^5)$
ε_D	0.000661	(0.0246, 0.0233)
E_D (psi)	46,199.18	$(3.24 \times 10^7, 3.23 \times 10^7)$

6.5. Model validation

The model shows a good tradeoff between the experimental results extracted from the published journals and simulation results captured using [12]. The correlation of FEA and experimental models are plotted and are as shown in **Figure 21** conforming the validation of the model.

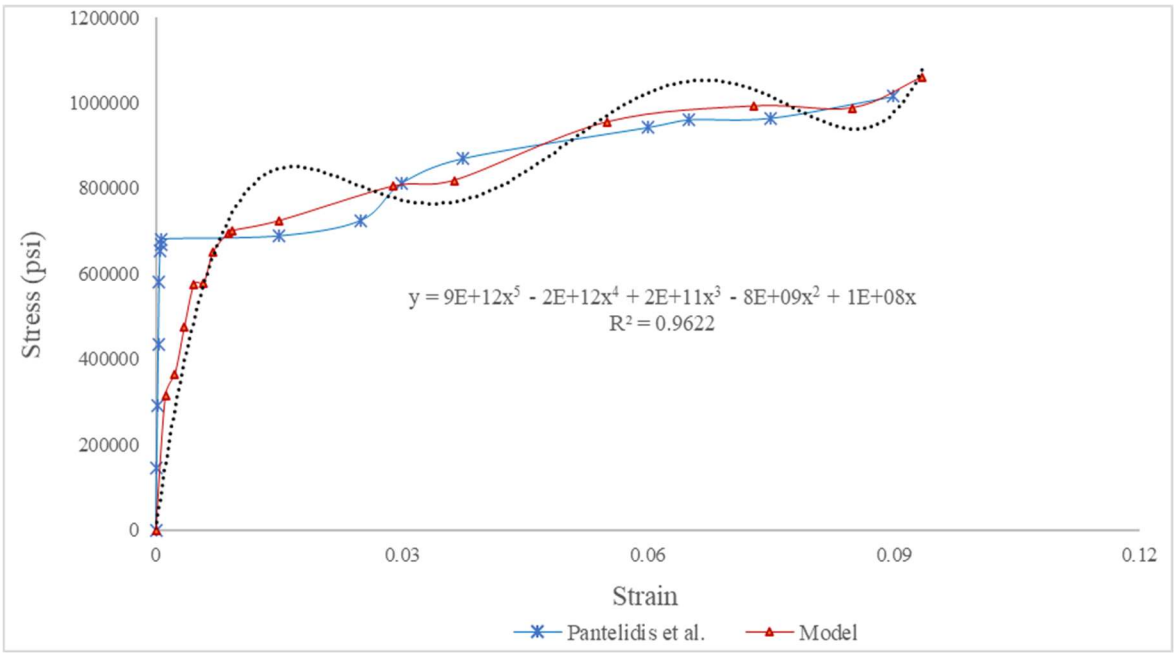

Figure 21. Model verification [12].

Figure 20 can decently provide a compatible and acceptable normalized stress and strain results data of the coupler composite at specific high strain rate load and high deformation incurred by semi-trailer impact via utilizing experimental and numerical results corresponding to the best fit curve with tight R^2 value of 0.96 as shown in Equation (14).

$$\sigma = 9 \times 10^{12} \times (\varepsilon^5) - 2 \times 10^{12} \times (\varepsilon^4) + 2 \times 10^{11} \times (\varepsilon^3) - 8 \times 10^9 \times (\varepsilon^2) + 10^8 \times (\varepsilon) \quad (18)$$

where: σ and ε indicate stress (in psi) and strain at coupler composite due to specific high strain rate loading to designate the overall material properties to safely withstand failure.

7. Discussions of results

Post impact performance of a coupler composite embedded in ABC bridge pier considering flexural response has been examined. Connectors consisting of splice-sleeve along with grouted coupler have been investigated for post impact performances. Stresses resulted due to impact and the amplification effect draw significant correlation between DIF_s computed analytically (1.053) and FEA (1.07) using the ratio of material properties at failure zones. In addition, results depicting from the mesh sensitivity studies are executed and results are shown in the respective **Figures 6–8** incorporating deformations and corresponding equivalent strain. Mesh sensitivity studies to incorporate static results are precisely shown in **Figure 6**, whereas the results from dynamic performance comprising deformation and strain for different mesh sizes are shown in **Figures 7** and **8** respectively. FEM analyses present a little conservative result as observed. To sum up the results, the following observations are drawn from this study:

1) Analytical results showing from the exaction solution comprises a DIF of 1.053 (i.e., increased by 5.3%). Using FEA, a DIF_s of 1.07 (i.e., 7% increment) has been estimated with an outcome of 1.6% increment. FEA results are used to determine and validate analytically computed DIF_s Provides a good agreement with a minimal difference in results (1.6%). This indicates high stress concentration in steel bar-coupler junction.
2) Due to the deployed boundary conditions for FEA, a little conservative result has been observed, and hence seems more realistic conforming design criteria. Results shown from the analytical solution provides a DIF_s of 1.053 (i.e., 5.3%), whereas material properties result a DIF_s of 1.07 (i.e., 7%) using dynamic properties of material.
3) This is observed from the results that maximum stress has developed at the contact of steel bar and coupler zone that leads high deformation. This is also observed that coupler and steel bar junction has been. Significant damage along with the bend and twist of steel bar has been observed in the junction as well.
4) Dynamic performances of the steel and concrete composite system and its post impact behavior are further assessed to precisely obtain stress and strain via developing linearized model and executing time dependent analyses.
5) Integrity analysis followed by reliability analysis using dynamic stress-strain resulted from simulations has been further carried out and the results are plotted through regression method. This can scrupulously capture material property at large post deformation state.
6) Model validation has been conducted using the results captured from static counterparts of stress and strain with the extracted experimental data. and is as shown in **Figure 20**.

8. Conclusions and future works

Bridge piers are usually contemplated as the most susceptible members to vehicle crash due to their exposed face and slender behavior. The characteristics and the associated severity of damage of the connectors used in ABC pier due to a high velocity and weight of semi-trailer collision were not well defined. Therefore, there

has been a dire need to verify the accountability of such existing structures against such collisions, and proffer solutions to limit such susceptibility to enhance its performance level. Based on the comparison of analytical studies and simulation results using FEA, and its validation with the experimental results published in the journals, the following conclusions can be drawn:

1) A reasonable enhancement in 7% to 10% strength of material modulus is recommended for the cast-iron and steel bar.
2) To precisely detect high variations of results due non-linearity, adequately accurate results are obtained through utilizing the integrity study.
3) By using CI, risk analysis has been conducted to provide a clear understanding to scrupulously using the uncertainty parameters.
4) High precision experimental studies are recommended before extensive use.

Table 9. US customary to the equivalent SI units.

US customary	SI unit
1 ksi	6.89 MPa (kN/mm^2)
1 ksi	6894.76 kN/m^2
1 kip-in	0.113 kN-m
1 kip	4.45 kN
1 lbs	0.00445 kN
1 mph	1.61 km/hr
1 ft-lb/s	0.00136 kN-m/s (1.36 N-m/s)
1 in	0.0254 m (25.4 mm)
1 foot	0.3048 m (304.80 mm)
1 pci	271.447 kN/m^3
1 psi	6894.76 N/m^2

The data conversions from US Customary to SI are shown in **Table 9**.

Funding: NMB Splice Sleeve Inc. North America and Utah State University, Logan, Utah 84322, United States.

Availability of data and material: Some or all data, models, or code that support the findings of this study are available from the corresponding author upon reasonable request.

Conflict of interest: The author declares no conflict of interest.

Abbreviations

f'_c	Concrete strength
A_g	Gross cross-sectional area of pier specimen
A_s	Cross-sectional area of reinforcing steel bar
A_{net}	Net cross-sectional area of pier
$A_{n,s}$	Cross-sectional area of each steel rebar
A_{CI}	Cross-sectional area of splice sleeve (cast iron)
A_{Grout}	Cross-sectional area of grout

$A_{connector}$	Cross-sectional area of hollow splice-sleeve
E_{CI}	Material modulus of cast iron
E_{Grout}	Material modulus of grout, concrete
$E_{Concrete}$	Material modulus of concrete
E_s	Material modulus of reinforcing steel rebar
η	Energy dissipation
f_y	Yield strength of steel
P_n	Axial load of RC pier
$P_{n,s}$	Axial load of reinforcing steel bar
$P_{n,s}$	Scaled-down design axial bar load
σ_{dyn}	Dynamic flow stress
σ_y	Static flow stress
$\acute{\varepsilon}$	Quasi-static strain rate of steel bar
h	Pier diameter
h_I	Height of impact from pier base
σ	Stress
ε	Strain
E	Modulus of elasticity of coupler
σ_D	Stress
ε_D	Strain
E_D	Modulus demand of coupler at dynamic impact
ψ	Dynamic parameter
C and p	Material constants
I_S	Static impact force
W	Vehicle weight
M_s	Static moment for each coupler
$M_{s,c}$	Static moment incurred by each coupler
$M_{dyn,c}$	Dynamic moment incurred by each coupler
M_{dyn}	Dynamic moment for each coupler
t	Impact duration (sec)
DIFs	Dynamic increase factor
CI	Confidence interval
μ	Mean
SD	Standard deviation
Z	Significance level
N	Sample size

References

1. Hauksson E, Kanamori H, Stock J, et al. Active Pacific North America Plate boundary tectonics as evidenced by seismicity in the oceanic lithosphere offshore Baja California, Mexico. Geophysical Journal International. 2013; 196(3): 1619-1630. doi: 10.1093/gji/ggt467
2. Thomas RJ, Steel K, Sorensen AD. Reliability analysis of circular reinforced concrete columns subject to sequential vehicular impact and blast loading. Engineering Structures. 2018; 168: 838-851. doi: 10.1016/j.engstruct.2018.04.099
3. Feyerabend M. Hard transverse impacts on steel beams and reinforced concrete beams. University of Karlsruhe (TH),

Germany; 1988.
4. Sharma H, Gardoni P, Hurlebaus S. Performance-Based Probabilistic Capacity Models and Fragility Estimates for RC Columns Subject to Vehicle Collision. Computer-Aided Civil and Infrastructure.
5. Roy S, Unobe I, Sorensen AD. Vehicle-Impact Damage of Reinforced Concrete Bridge Piers: A State-of-the Art Review. Journal of Performance of Constructed Facilities. 2021; 35(5): 03121001. doi: 10.1061/(ASCE)CF.1943-5509.0001613
6. Roy S, Unobe ID, Sorensen AD. Investigation of the performance of grouted couplers in vehicle impacted reinforced concrete ABC bridge piers. Advances in Bridge Engineering. 2022; 3(1). doi: 10.1186/s43251-022-00065-y
7. Sanders, David H. Evaluation of the Seismic Performance of Circular and Interlocking RC Bridge Columns under Bidirectional Shake Table Loading. In: Proceedings of the 15th World Conference on Earthquake Engineering (15WCEE); September 2018.
8. Pantelides CP, Ameli MJ, Parks JE, Brown DN. Seismic evaluation of grouted splice sleeve connections for precast RC bridge piers in ABC. Utah Department of Transportation; 2014.
9. Sharma H, Hurlebaus S, Gardoni P. Performance-based response evaluation of reinforced concrete columns subject to vehicle impact. International Journal of Impact Engineering. 2012; 43: 52-62. doi: 10.1016/j.ijimpeng.2011.11.007
10. Kowalsky MJ. Deformation limit states for circular reinforced concrete bridge columns. Journal of Structural Engineering, American Society of Civil Engineers. 126(8); 869-878. doi: 10.1061/(ASCE)0733-9445(2000)126:8(869)
11. Roy S, Unobe ID, Sorensen A. Damage characterization and resilience optimization of reinforced concrete bridge piers under vehicle impact. Advances in Bridge Engineering. 2022; 3(1). doi: 10.1186/s43251-022-00067-w
12. Ameli MJ, Brown DN, Parks JE, et al. Seismic Column-to-Footing Connections Using Grouted Splice Sleeves. ACI Structural Journal. 2016; 113(5). doi: 10.14359/51688755.
13. Jacob GC, Fellers JF, Starbuck JM, et al. Crashworthiness of automotive composite material systems. Journal of Applied Polymer Science. 2004; 92(5): 3218-3225. doi: 10.1002/app.20336
14. Ebrahimpour A, Earles B. Seismic Performance of Columns with Grouted Couplers in Idaho Bridges. IABSE Symposium, Vancouver 2017: Engineering the Future. 2017; 109: 1817-1823. doi: 10.2749/vancouver.2017.1817
15. Tazarv M, Saiidi MS. Seismic design of bridge columns incorporating mechanical bar splices in plastic hinge regions. Engineering Structures. 2016; 124: 507-520. doi: 10.1016/j.engstruct.2016.06.041
16. Zhao X, Wu YF, Leung AY, et al. Plastic Hinge Length in Reinforced Concrete Flexural Members. Procedia Engineering. 2011; 14: 1266-1274. doi: 10.1016/j.proeng.2011.07.159
17. Roy S, Sorensen A. Energy Based Model of Vehicle Impacted Reinforced Bridge Piers Accounting for Concrete Contribution to Resilience. In: Proceedings of the 18th International Probabilistic Workshop: IPW 2020. p. 301.
18. Roy S, Sorensen A. A Reliability Based Crack Propagation Model for Reinforced Concrete Bridge Piers Subject to Vehicle Impact. In: Proceedings of the 18th International Probabilistic Workshop: IPW 2020. p. 95.
19. ACI. ACI 318-11: Building Code Requirements for Structural Concrete. American Concrete Institute; 2011.
20. ICC-ES Evaluation Report ESR-3433. Available online: https://icc-es.org/report-listing/esr-3433/ (accessed on 2 March 2024).
21. ICC-ES Report. Available online: https://www.pwcva.gov/assets/2021-05/PA1201Att (accessed on 2 March 2024).
22. Gray GT. High-Strain-Rate Deformation: Mechanical Behavior and Deformation Substructures Induced. Annual Review of Materials Research. 2012; 42(1): 285-303. doi: 10.1146/annurev-matsci-070511-155034
23. Chopra AK. Dynamics of Structures, Theory and Applications to Earthquake Engineering. Upper Saddle River: Pearson-Prentice Hall; 2001.
24. Wikipedia. Speed limits in the United States. Available online: https://en.wikipedia.org/wiki/Speed_limits_in_the_United_States (accessed on 2 June 2024).
25. Tavio T, Tata A. Predicting Nonlinear Behavior and Stress-Strain Relationship of Rectangular Confined Reinforced Concrete Columns with ANSYS. Civil Engineering. 2009; 11(1): 23-31.
26. Malvar LJ. Review of static and dynamic properties of steel reinforcing bars. ACI Materials Journal.
27. Malvar LJ, Crawford JE. (1998). Dynamic increase factors for steel reinforcing bars. 28th DDESB Seminar.
28. Buth CE, Brackin MS, Williams WF, Fry GT. Collision Loads on Bridge Piers: Phase 2 Report of Guidelines for Designing Bridge Piers and Abutments for Vehicle Collisions. Austin, Texas. 2011; p. 100.
29. Cowper GR, Symonds PS. Strain-hardening and strain-rate effects in the impact loading of cantilever beams. Defense Technical Information Center; 1957. doi: 10.21236/ad0144762

30. AFDC. Vehicle Weight Classes & Categories. Alternative Fuels Data Centre, U.S. Department of Energy; 2018.
31. Roy S. Sustainability and Resiliency Investigation of Grouted Coupler Embedded in RC ABC Bridge Pier at Vehicle Impact. Engineering and Applied Sciences. 2024; 9(1): 14-33. https://doi.org/10.11648/j.eas.20240901.12
32. Ameli MJ, Pantelides CP. Seismic analysis of precast concrete bridge columns connected with grouted splice sleeve connectors. Journal of Structural Engineering, American Society of Civil Engineers. 2017; 143(2): 4016176. doi: 10.1061/(ASCE)ST.1943-541X.0001678
33. Andrzej S, Nowak KR, Collins. Reliability of Structures, 2nd ed. CRC Press; 2012.
34. El-Tawil S, Severino E, Fonseca P. Vehicle collision with bridge piers. Journal of Bridge Engineering. 2005; 10(3): 345-353.
35. Matos JC, Lourenço PB, Oliveira DV, et al. 18th International Probabilistic Workshop. Springer International Publishing; 2021.